Materials Letters 273 (2020) 127928

Contents lists available at ScienceDirect

Materials Letters

journal homepage: www.elsevier.com/locate/mlblue

One-step hydrothermal synthesis of three-dimensional structures of MoS_2/Cu_2S hybrids via a copper foam-assisted method

Zhiying Chen [a], Yijian Liang [a,b], Aiping Liu [c], Yanhui Zhang [a], Yanping Sui [a], Shike Hu [a,b], Jing Li [a,b], He Kang [a,b], Shuang Wang [a,b], Sunwen Zhao [a,b], Guanghui Yu [a,*]

[a] State Key Laboratory of Functional Materials for Informatics, Shanghai Institute of Microsystem and Information Technology (SIMIT), Chinese Academy of Sciences, 865 Changning Road, Shanghai 200050, China
[b] University of Chinese Academy of Sciences, No. 19A Yuquan Road, Beijing 100049, China
[c] Center for Optoelectronics Materials and Devices, Key Laboratory of Optical Field Manipulation of Zhejiang Province, Zhejiang Sci-Tech University, Hangzhou 310018, China

ARTICLE INFO

Article history:
Received 22 February 2020
Received in revised form 30 April 2020
Accepted 2 May 2020
Available online 4 May 2020

Keywords:
Microstructure
Surfaces
Crystal growth

ABSTRACT

Recent studies proved that MoS_2 is a promising noble metal-free electrocatalyst for hydrogen evolution reaction. Here, we report the three-dimensional (3D) structures of MoS_2/Cu_2S hybrids were prepared by a one-step hydrothermal method using copper foam. Cu_2S derived from the copper foam was used as the self-template of the 3D structures. The MoS_2 nanosheet arrays were vertically aligned on the surface of Cu_2S networks. The MoS_2 nanosheets on the 3D Cu_2S structure maximized the exposure of their edge sites at the atomic scale and presented superior catalysis activity for hydrogen production. The ease of composite fabrication suggested that the MoS_2/Cu_2S composite is a promising candidate electrode material for hydrogen evolution.

1. Introduction

Hydrogen is regarded as a promising replacement for traditional petroleum fuels in the future. The electrolysis of water can be an important and environmentally friendly pathway for hydrogen production. Hence, hydrogen production from water splitting has attracted growing attention [1–5]. Noble metal catalysts, such as Pt, Ru, and Ir, are the most effective catalysts for hydrogen evolution reaction (HER). Although these noble metals exhibit excellent electrocatalytic activity and the lowest overpotential for HER, their scarcity and high cost limit their applications [6]. Therefore, extensive efforts have been carried out to develop noble metal-free electrocatalysts.

Transition metal dichalcogenide (TMDs) have been recognized as low-cost catalyst alternatives for HER reaction because of their highly catalytic activity [7–9]. The most extensively studied TMD material is MoS_2 because of its electrocatalyst properties and natural abundance [10]. The catalytic performance of MoS_2 for HER mainly relies on catalytic site numbers (defects at edges or planes) and efficient exposure surfaces. The exposure surfaces are closely associated with microstructures and nanostructures at electrodes (e.g., vertical nanosheet arrays) [11]. However, prepared MoS_2 layers tend to aggregate during practical application, resulting in the loss of active sites [12]. To date, the preparation of MoS_2 composites is an important strategy to improve the catalytic activity of MoS_2 [21–23]. In this paper, we report for the first time the use of Cu_2S derived from copper foam as a self-template of 3D MoS_2/Cu_2S structures in a one-step hydrothermal synthesis, in which MoS_2 nanosheet arrays are vertically aligned on the surface of Cu_2S networks.

2. Methods and materials

All chemical reagents used in the experiment were of analytical grade and were not subjected to further purification.

Preparation of MoS_2: 1 mmol of ammonium molybdate tetrahydrate ($(NH_4)_6Mo_7O_{24}{\cdot}4H_2O$) and 30 mmol of thiourea ($SC(NH_2)_2$) were dissolved in 35 mL of deionized water. The homogeneous dispersion was transferred into a Teflon-lined autoclave (50 mL) and heated at 180 °C for several hours.

Preparation of Cu_2S: 30 mmol of thiourea ($SC(NH_2)_2$) were dissolved in 35 mL of deionized water. A piece of Cu foam (1 cm × 1 cm × 0.1 cm) was reduced in an H_2 flow of 500 sccm at 1050 °C for 10 min. Then the homogeneous dispersion and the hydrogen-reduced Cu foam were transferred into a Teflon-lined autoclave (50 mL), and heated at 180 °C for several hours.

* Corresponding author.
E-mail address: ghyu@mail.sim.ac.cn (G. Yu).

https://doi.org/10.1016/j.matlet.2020.127928
0167-577X/

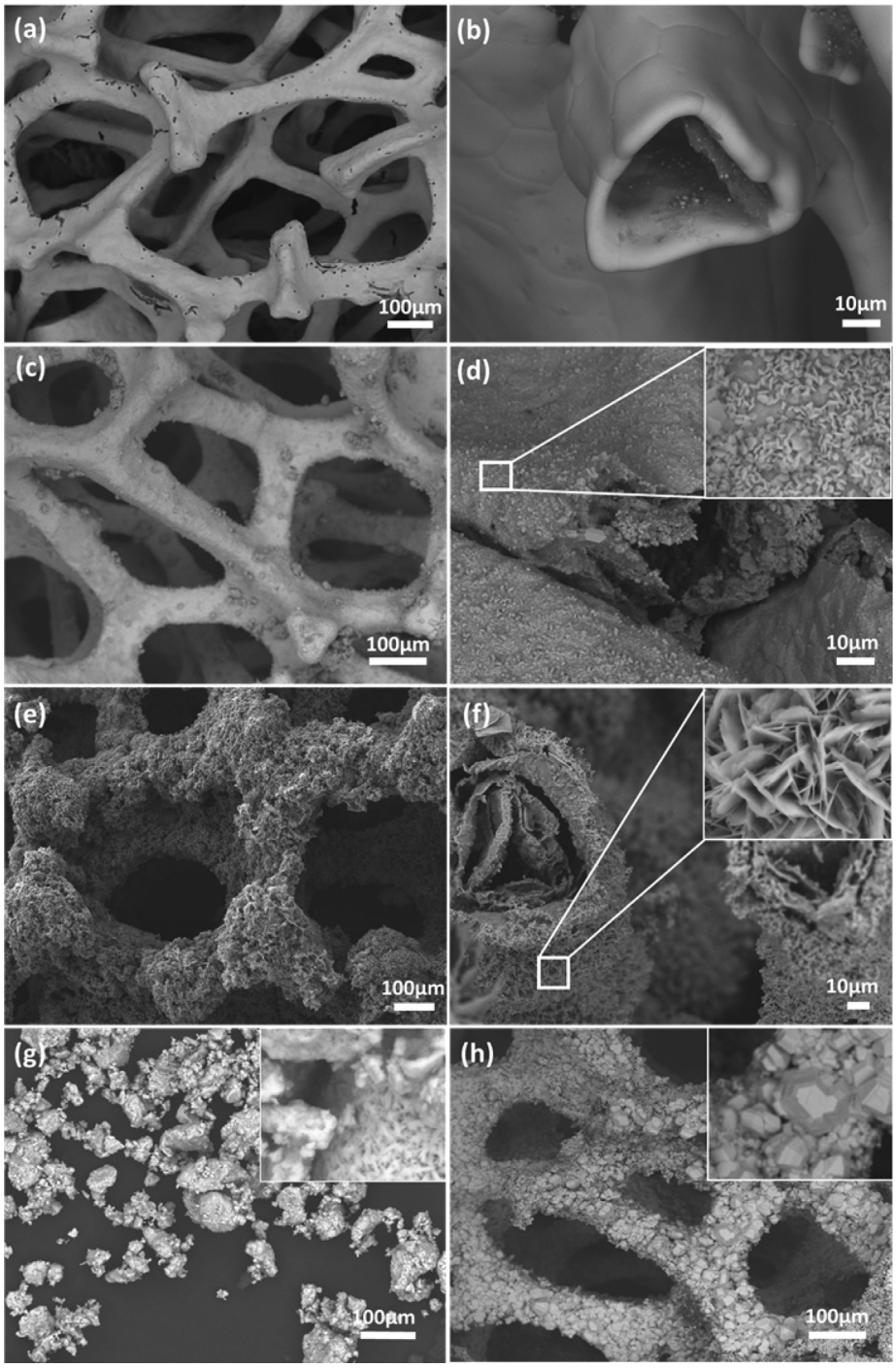

Fig. 1. FESEM images of (a) Cu foam and (b) hollow structure of Cu foam. (c, e) Low-magnification FESEM images of MoS_2/Cu_2S growing for 8 and 24 h, (d and f) cross-sectional view of FESEM images of (c) and (e). The insets of (d) and (f) show the high-magnification FESEM images of MoS_2/Cu_2S. (g, h) Low-magnification FESEM images of MoS_2 power and 3D Cu_2S. The insets of (g) and (h) show the high-magnification FESEM images of MoS_2 power and 3D Cu_2S.

Preparation of MoS_2/Cu_2S hybrids: 1 mmol of ammonium molybdate tetrahydrate ($(NH_4)_6Mo_7O_{24}{\cdot}4H_2O$) and 30 mmol of thiourea ($SC(NH_2)_2$) were dissolved in 35 mL of deionized water. A piece of Cu foam (1 cm × 1 cm × 0.1 cm) was reduced in an H_2 flow of 500 sccm at 1050 °C for 10 min. Then the homogeneous dispersion and the hydrogen-reduced Cu foam were transferred into a Teflon-lined autoclave (50 mL), and heated at 180 °C for several hours.

The obtained solid products (MoS_2 power, 3D Cu_2S and 3D MoS_2/Cu_2S hybrids) was washed several times with deionized water and ethanol for several times, and then dried in a vacuum oven at 60 °C for 12 h.

A saturated calomel electrode (SCE) and a graphite rod were used as the reference electrode and counter electrode, respectively. The produced 3D Cu_2S or MoS_2/Cu_2S composite was used as the working electrode. The produced MoS_2 power (3 mg was needed) and 120 μL Nafion solution (5 wt%) were dispersed in a 1.5 mL water-ethanol solution with volume ratio of (3:1) and sonicated for 0.5 h to form a homogeneous ink. Then 5 μL of the suspension was drop-casted onto the glassy carbon electrode (GCE) surface.

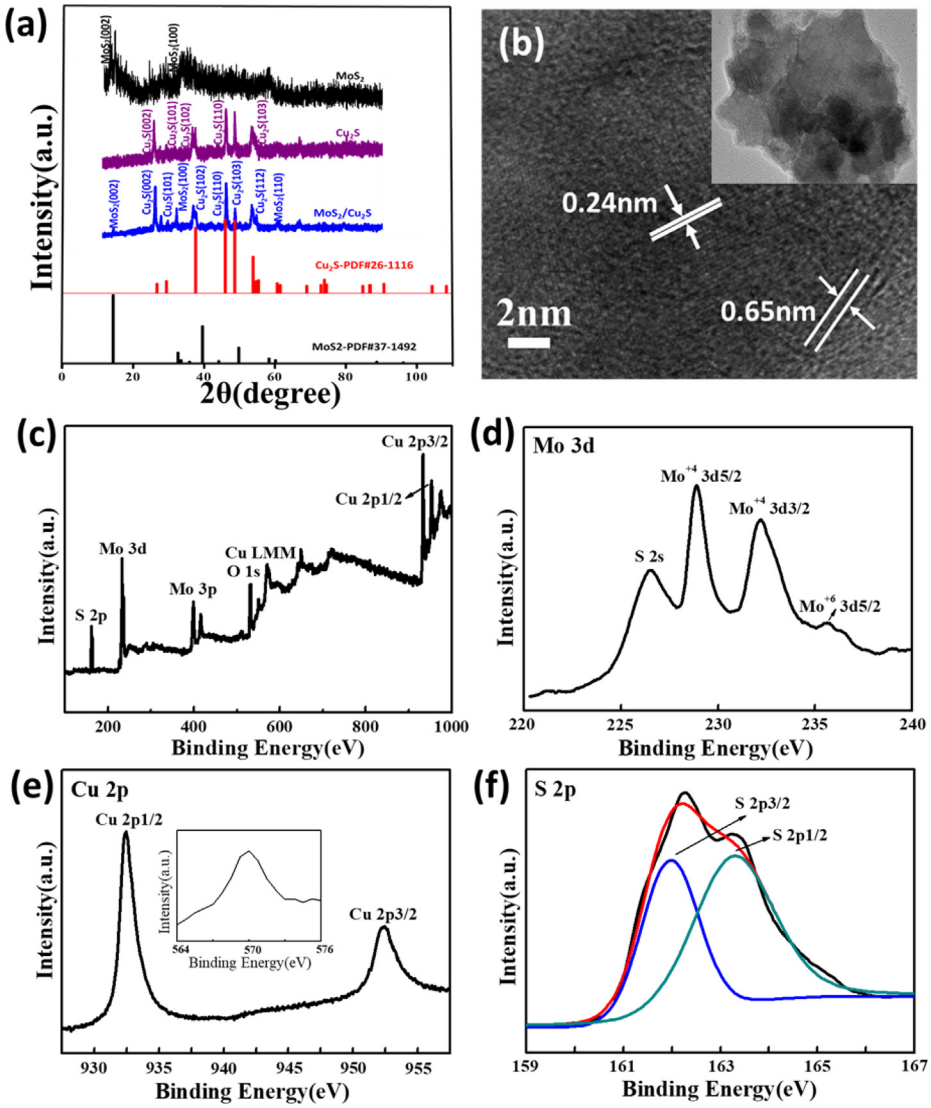

Fig. 2. (a) XRD patterns of MoS_2, Cu_2S and MoS_2/Cu_2S, respectively. (b) HRTEM images of as-prepared 3D MoS_2/Cu_2S structure grown for 24 h, and (c) XPS survey spectra of MoS_2/Cu_2S, (d–f) XPS spectra of Mo 3d, Cu 2p, and S 2p.

Linear sweep voltammetry (LSV) measurement with a scan rate of 5 mV/s was conducted in a 0.5 M H_2SO_4 (purged in pure N_2 for 30 min before activity test).

Scanning electron microscopy (SEM) was performed using a HITACHI TM-1000 scanning electron microanalyzer. X-ray photoelectron spectroscopy characterization (XPS, Axis Ultra) was utilized to characterize elemental composition. High-resolution TEM (HRTEM) and selected area electron diffraction were performed on a JEOL 2100F with a beam energy of 200 keV. X-ray diffraction (XRD) was conducted using a DX-2700A X-ray diffractometer (Precision Instruments Co. Ltd, Shanghai, China). All electrochemical measurements were conducted on a CHI 660D electrochemical workstation (Shanghai Chenhua Instrument Co., China) in a three-electrode cell at room temperature.

3. Results and discussion

The MoS_2 grown on the 3D structures of Cu_2S in the hydrothermal synthesis involved three key steps based on the common knowledge of sulfur compounds and the published literature [14]. First, the MoS_2 nuclei was rapidly formed via the redox reactions of H_2S (from the hydrolysis of CSN_2H_4 in Eq. (1)) with MoO_4^{2-} (from the ionization of $(NH_4)_6Mo_7O_{24}$), as shown in Eq. (2).

$$NH_2CSNH_2 + 2H_2O \rightarrow 2NH_3 + H_2S + CO_2 \quad (1)$$

$$4MoO_4^{2-} + 9S^{2-} + 24H^+ \rightarrow 4MoS_2 + SO_4^{2-} + 12H_2O \quad (2)$$

The MoS_2 nuclei grew into nano-plates according to the crystal growth habit. The MoS_2 nano-plates were then convoluted to form a larger flowerlike structure. In the hydrothermal process, the hollow copper was separated by several layers, and the copper foam was vulcanized, consequently forming cuprous sulfide. The formed MoS_2 was arranged vertically on the surface of different layers of the Cu_2S structures.

The morphologies of the 3D MoS_2/Cu_2S, 3D CuS_2 and MoS_2 power were confirmed by SEM, as shown in Fig. 1. The porous copper foam surfaces and the hollow structure are shown in Fig. 1(a, b). After 8 h of hydrothermal reaction, the Cu_2S substrate was covered by MoS_2 nanosheets. The inset of Fig. 1(d) shows that the as-grown MoS_2 nanosheets were vertically and sparsely arranged on the surface of the Cu_2S substrate. The arrangement of MoS_2 was intensive, and the size of the MoS_2 nanosheets increased with time from 8 h to 24 h, as shown in Fig. 1(e, f). The hollow Cu_2S tube was

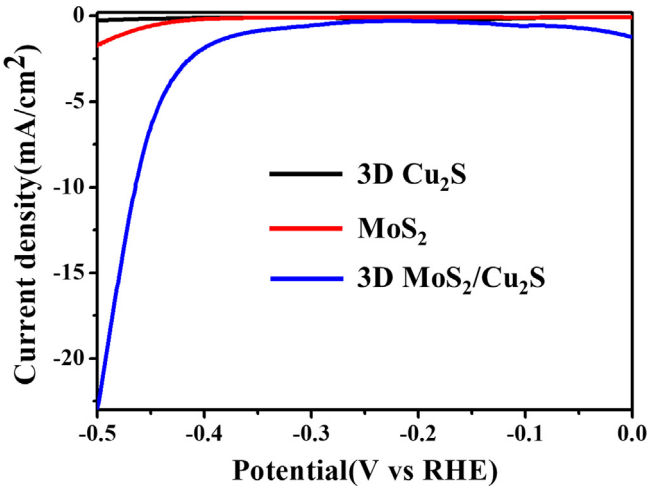

Fig. 3. Polarization curves of pure 3D Cu_2S, MoS_2, and MoS_2/Cu_2S hybrids grown for 24 h.

separated by several layers, the formation of the multilayer Cu_2S was attributed to the volume expansion during the transformation of Cu into Cu_2S, and the number of layers increased with time. The morphology of MoS_2 power was shown in Fig. 1(g). We can see from the picture that the dispersion of MoS_2 power is poor and the size is not uniform. Cu foam promotes the dispersion of MoS_2 nanosheets and increases the surface area. The 3D Cu_2S synthesized by hydrothermal process is shown in Fig. 1(h). The inset of Fig. 1(h) shows that the 3D Cu_2S is composed of block structure. Comparing Fig. 1(h), (d) and (f), we have reason to speculate that the MoS_2 covering on the surface inhibits the formation of block Cu_2S.

XRD was performed to study the structure of MoS_2, Cu_2S and MoS_2/Cu_2S, and the results are shown in Fig. 2(a). The well-defined peaks of Cu_2S can be well-indexed to the face-centered cubic Cu_2S (JCPDS no. 26-1116) [13]. The XRD peaks pertaining to MoS_2 revealed the hexagonal phase of MoS_2 (JCPDS no. 37-1492). As presented in Fig. 2(a), MoS_2 showed peaks at $2\theta = 14.1°$, 33.8°, and 59.3°, which can be indexed to the (0 0 2), (1 0 0), and (1 1 0) planes, respectively. The peak at 14.1° corresponded to the c-plane of MoS_2. The weakness of the peak (14.1°) indicated that the MoS_2 nanosheets might have comprised only a few layers and were thus too thin to detect anything but the weak peak [15]. HRTEM were employed to further confirm the structure and morphology of the Cu_2S/MoS_2 composite. The image shown in Fig. 2(b) displays slices consisting of a bi-component of MoS_2 and Cu_2S. The interlayer fringes of the selected area were 0.65 and 0.24 nm, which agreed well with the (0 0 2) plane of MoS_2 and the (1 1 0) plane of Cu_2S, respectively. Comprehensive information on the surface electronic state and chemical composition of MoS_2/Cu_2S composites can be further provided by XPS measurements, as shown in Fig. 2(c–f). The wide scan XPS spectra of the MoS_2/Cu_2S composites (Fig. 2c) clearly indicated that the sample was composed of Mo, Cu, S, and O elements and that no peaks of other elements were observed. High-resolution Mo 3d spectrum (Fig. 2d) showed characteristic peaks centered at 232.3 and 229.2 eV and corresponded to Mo 3d3/2 and Mo 3d5/2 orbitals, respectively. This result suggested that Mo in the MoS_2/Cu_2S hybrid was the Mo^{+4} state. In addition, the peak at 235.2 eV corresponded to a small amount of unreacted MoO_3 on the surface of MoS_2 [16]. Similarly, the broad peak in Fig. 2(f) shows the S 2p spectrum, which, on further deconvolution, revealed the presence of peaks at 161.7 and 163.2 eV that respectively indicated the presence of S 2p3/2 and S 2p1/2 levels [17]. In addition, the peaks at 932.4 eV (Cu 2p3/2) and 952.4 eV (Cu 2p1/2) confirmed the formation of monovalent copper sulfide (chalcocite), which is consistent with the NIST XPS database. The presence of an auger peak at 569.6 eV, as depicted in Fig. 2(e), indicated the presence of copper in (I) state and validated the formation of Cu_2S. Moreover, the absence of any satellite peaks in the Cu 2p spectra implied that the synthesized material was devoid of other crystallographic phases of copper [18–20].

We further explored the activity of the hybrids toward HER in 0.5 M H_2SO_4 using a three electrode electrochemical cell. The electrochemical polarization curves plotted in Fig. 3 confirm that the hybrid materials improved the HER catalysts relative to pure MoS_2 particles or 3D Cu_2S at an overpotential of −0.42 V.

4. Conclusions

In summary, we present a one-step hydrothermal method to prepare MoS_2/Cu_2S hybrids with vertically aligned MoS_2 nanosheets grown on 3D Cu_2S structures. Cu_2S derived from copper foam is used as the self-template of the 3D structures. The vertically oriented nanosheets grown on the surface of the layered Cu_2S not only increase the density of active sites but also decrease the charge transfer resistance during the HER process. As a result, the 3D MoS_2/Cu_2S hybrids exhibit better activity in acid media in comparison with pure MoS_2 particles and 3D Cu_2S.

CRediT authorship contribution statement

Zhiying Chen: Designing experiment, Writing- Original draft preparation. **Yijian Liang:**Analysis of samples by XRD. **Aiping Liu:** Electrical testing of samples. **Yanhui Zhang:** Investigation. **Yanping Sui:** Investigation. **Editing Shike Hu:** Investigation. **Jing Li:** Methodology. **He Kang:** Data curation. **Shuang Wang:** Analysis of samples by XPS. **Sunwen Zhao:** Software. **Guanghui Yu:** Reviewing and Editing.

Declaration of Competing Interest

The authors declare that they have no known competing financial interests or personal relationships that could have appeared to influence the work reported in this paper.

Acknowledgements

This work was supported by National defense technology innovation special zone project and the National Natural Science Foundation of China (No. 51402342). This work was financially supported by the Science and Technology Commission of Shanghai Municipality (18511110700).

References

[1] J.A. Turner, Science 305 (2004) 972–974.
[2] K. Ikeue, Y. Shinmura, M. Machida, Appl. Catal. B: Environ. 123 (2012) 84–88.
[3] F. Zhang, K. Maeda, T. Takata, K. Domen, J. Catal. 280 (2011) 1–7.
[4] N. Singh, J. Hiller, H. Metiu, Electrochim. Acta 145 (2014) 224–230.
[5] C.G. Morales-Guio, L.A. Stern, X. Hu, Chem. Soc. Rev. 43 (2014) 6555–6569.
[6] R. Subbaraman, D. Tripkovic, D. Strmcnik, K.C. Chang, M. Uchimura, A.P. Paulikas, V. Stamenkovic, N.M. Markovic, Science 334 (2011) 1256–1260.
[7] I. Bilgin, F.Z. Liu, A. Vargas, A. Winchester, M.K.L. Man, M. Upmanyu, K.M. Dani, G. Gupta, S. Talapatra, A.D. Mohite, S. Kar, ACS Nano 9 (2015) 8822–8832.
[8] H. Wang, D. Kong, P. Johanes, J.J. Cha, G. Zheng, K. Yan, N. Liu, Y. Cui, Nano Lett. 13 (2013) 3426–3433.
[9] J. Zhang, S.H. Liu, H.W. Liang, R.H. Dong, X.L. Feng, Adv. Mater. 27 (2015) 7426–7431.
[10] M. Chhowalla, H.S. Shin, G. Eda, L.J. Li, K.P. Loh, H. Zhang, Nat. Chem. 5 (2013) 263–275.
[11] X.S. Chen, G.B. Liu, W. Zheng, W. Feng, W.W. Cao, W.P. Hu, P.A. Hu, Adv. Funct. Mater. 26 (2016) 8537–8544.
[12] K. Chang, W. Chen, L. Ma, H. Li, F. Huang, Z. Xu, Q. Zhang, J. Lee, J. Mater. Chem. 21 (2011) 6251–6257.

[13] S. Mao, Z. Wen, S. Ci, X. Guo, K. Ostrikov, J. Chen, Small 11 (2015) 414–419.
[14] T. Sun, Z. Li, X. Liu, L. Ma, J. Wang, S. Yang, J. Power Sources 331 (2016) 180–188.
[15] K. Chang, W.X. Chen, J. Mater. Chem. 21 (2011) 17175–17184.
[16] Y. Kim, D.H. Jackson, D. Lee, M. Choi, T.W. Kim, S.Y. Jeong, H.J. Chae, H.W. Kim, N. Park, H. Chang, T.F. Kuech, Adv. Funct. Mater. 27 (2017) (1834) 1701825–1702170.
[17] D. Barrera, Q. Wang, Y.J. Lee, L. Cheng, M.J. Kim, J. Kim, J.W. Hsu, J. Mater. Chem. C 5 (2017) 2859–2864.
[18] X. Wang, F. Lv, T. Li, Y. Han, Z. Yi, M. Liu, J. Chang, C. Wu, ACS Nano 11 (2017) 11337–11349.
[19] M. Ye, C. Chen, N. Zhang, X. Wen, W. Guo, C. Lin, Adv. Energy Mater. 4 (2014) 1301564–1301571.
[20] P. Sahatiya, A. Kadu, H. Gupta, P.T. Gomathi, S. Badhulika, ACS Appl Mater. Interfaces. 10 (2018) 9048–9059.
[21] J.H. Jian, Y. Li, H. Bi, X.Z. Wang, X.H. Wu, W. Qin, ACS Sustainable Chem. Eng. 8 (2020) 4547–4554.
[22] Z.X. Zhang, Y.X. Wang, X.X. Leng, V.H. Crespi, F.Y. Kang, R.T. Lv, ACS Appl. Energy Mater. 1 (2018) 1268–1275.
[23] J.M. Cao, J. Zhou, Y.F. Zhang, Y.X. Wang, X.W. Liu, ACS Appl. Mater. Interfaces 10 (2018) 1752–1760.